Journal of Power Sources 191 (2009) 495–500

Contents lists available at ScienceDirect

Journal of Power Sources

journal homepage: www.elsevier.com/locate/jpowsour

Anticorrosion properties of Ta-coated 316L stainless steel as bipolar plate material in proton exchange membrane fuel cells

Haijun Yu*, Lijun Yang, Lei Zhu, Xuyu Jian, Zhong Wang, Lijun Jiang

Department of Energy Material and Technology, Beijing General Research Institute for Nonferrous Metals, Beijing, 100088, China

ARTICLE INFO

Article history:
Received 9 January 2009
Received in revised form 6 February 2009
Accepted 6 February 2009
Available online 20 February 2009

Keywords:
Proton exchange membrane fuel cell (PEMFC)
Bipolar plate
316L stainless steel (SS316L)
Tantalum (Ta)
Corrosion current density

ABSTRACT

In order to reduce the cost, volume and weight of the bipolar plates used in the proton exchange membrane fuel cells (PEMFC), more attention is being paid to metallic materials, among which 316L stainless steel (SS316L) is quite attractive. In this study, metallic Ta is deposited on SS316L using physical vapor deposition (PVD) to enhance the corrosion resistance of the bipolar plates. Simulative working environment of PEMFC is applied for testing the corrosion property of uncoated and Ta-coated SS316L. X-ray diffraction (XRD), scanning electron microscopy (SEM) and electrochemical methods (potentiodynamic and potentiostatic polarization) are also used for analyzing characteristics of uncoated and Ta-coated SS316L. Results show that, Ta-coated SS316L has significantly better anticorrosion property than that of uncoated SS316L, with corrosion current densities of uncoated SS316L being 44.61 $\mu A\,cm^{-2}$ versus 9.25 $\mu A\,cm^{-2}$ for Ta-coated SS316L, a decrease of about 5 times. Moreover, corrosion current densities of Ta-coated SS316L in both simulative anode (purged with H_2) and cathode (purged with air) conditions are smaller than those of uncoated SS316L.

1. Introduction

With the increasing concern of energy and environment, more attention is being paid to new alternative energy technologies, such as hydrogen fuel cells. Proton exchange membrane fuel cell (PEMFC), using H_2 as a fuel, is one of the most important fuel cells, because it offers high energy efficiency and high specific power, is environmentally friendly, has a long life, and easy start-up at low temperatures. So PEMFC is not only a good potential for use in powering distributed power stations, but also suitable for mobile power supplies. Therefore, it is an ideal candidate for electric vehicles (EV) and hybrid-electric vehicles (HEV) as well as an optimal home power system [1–5].

The bipolar plate is one of the key elements of PEMFC. It is a multi-functional component, which is used to collect the current, in distributing fuel and oxygen, in separating of individual cells, and to facilitate water and heat management. Currently, graphite is material of choice for producing commercial bipolar plates due to its low interface resistance, good anticorrosion properties, and high electrical conductivity. However, graphite is brittle and permeable to gases, so graphite bipolar plates are commonly very thick (more than 3 mm). In addition, the cost of PEMFC is about US$200 kW^{-1}, and the cost of a graphite bipolar plate is about US$90 kW^{-1} [6], accounting for about 45% of the cost and 80% of the weight of the PEMFC stack [4], which is too expensive for commercial application. Hence, the key to increasing the application of PEMFC is to decrease their cost, weight and volume. Considerable attention is recently given to metallic bipolar plates for their superior manufacturability, durability to shocks and vibration, no permeability and cost effectiveness when compared with graphite-based materials. The thinnest bipolar plate using metal can be 0.1 mm [7], so the total weight, volume and cost of metallic bipolar plate can be largely decreased. However, the main handicap of metallic bipolar plate is the lack of ability to combat corrosion in aggressive acidic and humid working environment of PEMFC. Therefore, the determination of a suitable metal with increased anticorrosion properties is the main focus of current research efforts. Corrosion properties of various metals and alloys as well as various coated materials are under researching in PEMFC working environment [8–15].

SS316L has the fine mechanical property, low cost and good anticorrosion property, while metallic Ta has significant anticorrosion property in sulfur acid environment, so SS316L with Ta coating has been chosen as the researching material. Physical vapor deposition (PVD) is one of the most promising coating technologies and is widely used for improvement of the mechanical, wear and corrosion properties, which is used for coating Ta on SS316L in this paper [8]. Furthermore, based on the cost analysis of metallic bipolar plate plus coating by Tawfik et al. [6], the cost of Ta-coated SS316L material will be less than US$20 kW^{-1}. In this study, the anticorrosion properties of uncoated and Ta-coated SS316L materials in

* Corresponding author. Tel.: +86 10 82241239; fax: +86 10 82241239.
E-mail address: yuhaijunneu@163.com (H. Yu).

0378-7753/$ – see front matter © 2009 Elsevier B.V. All rights reserved.
doi:10.1016/j.jpowsour.2009.02.020

Table 1
Chemical composition of SS316L (wt%).

Metal	Ni	Cr	Mo	Mn	C	P	S	Si	Cu	N	Fe
SS316L	10.81	16.45	2.04	1.49	0.022	0.028	0.01	0.34	0.45	0.03	Balance

0.5 mol dm^{-3} H_2SO_4 at 70 °C and simulative working environments (the applied potential being −0.1 V versus SCE purged with H_2 at the anode; and the applied potential being 0.6 V versus SCE purged with air at the cathode [6]) were investigated.

2. Experiment

2.1. Base material and PVD coating

The SS316L was first cut into specimens of Φ10 mm × 3 mm (area = 0.785 cm^2). Prior to PVD coating, the specimens were polished on 240, 500, and 800 grit silicon carbide papers and then finally polished on a polishing machine. The uncoated specimens were polished on 240, 600, 800 and 1000 grit silicon carbide papers. The coating process utilized was physical vapor deposition technology, which was used to apply metallic Ta on one side of the material. The chemical analysis of SS316L used in this study is given in Table 1.

2.2. Characterization

Surface characterizations of coated and uncoated SS316L before and after being corroded were described with Hitachi S4800 scanning electron microscopy (SEM) and the structures of uncoated and Ta-coated SS316L were characterized by X-ray diffraction (XRD) (Philips APD-10).

2.3. Electrochemical testing

Before electrochemical testing, one side of specimen was electrical contacted with copper wire using spot welding, and then the edges of specimen were sealed with epoxy resin. Potentiodynamic tests using Princeton Applied Research 2273 were chosen in order to analyze the corrosion results of uncoated and Ta-coated SS316L specimens. In the potentiodynamic tests, the initial potential was −0.25 V versus open circuit potential (OCP), the final potential was 1.3 V versus SCE, and the scan rate was 1 mV s^{-1}.

For the purpose of simulating actual working conditions of PEMFC [6], potentiostatic tests were chosen. At the anode, the applied potential was −0.1 V versus SCE purged with H_2, at the cathode, the applied potential was 0.6 V versus SCE purged with air, and the temperature and electrolyte were 70 °C and 0.5 mol dm^{-3} H_2SO_4 respectively.

3. Results and discussion

3.1. Characterization of uncoated and Ta-coated SS316L

3.1.1. SEM analysis of uncoated and Ta-coated SS316L

Fig. 1 is the SEM micrograph of Ta-coated SS316L. Fig. 1a shows the surface of Ta-coating, from which it can be clearly seen that the surface of Ta-coating is flat and smooth, with no pores or

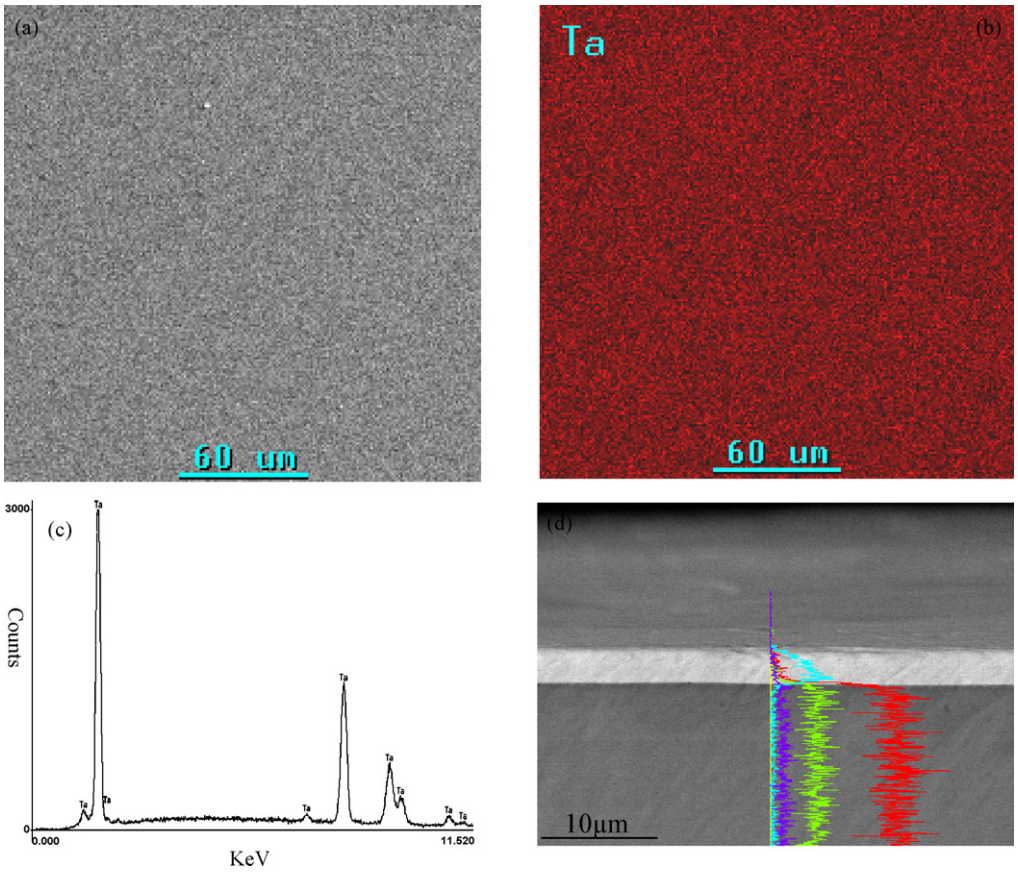

Fig. 1. Ta-coated SS316L (a) Ta coating surface, (b) backscattering electron image of Ta element, (c) superficial scanning EDX analysis, and (d) cross-sectional micrograph.

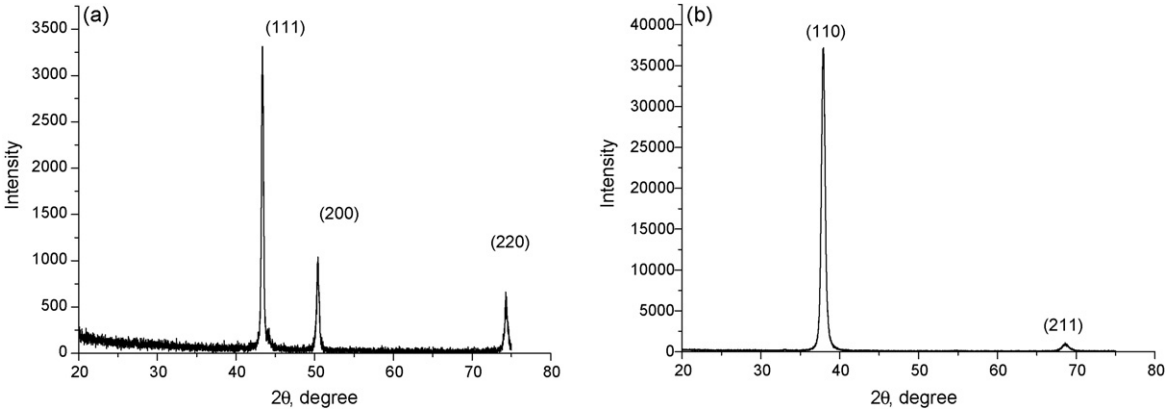

Fig. 2. XRD patterns for (a) uncoated and (b) Ta-coated SS316L.

cracks. In the interest of elemental distribution and composition on the surface of Ta-coated SS316L, backscattering and energy dispersive X-ray (EDX) analyses were also conducted. Fig. 1b shows the backscattering electron image, where the Ta-coating distribution on the surface of SS316L can be seen. Note that the Ta element is homogeneously distributed on the surface. Superficial scanning EDX analysis of Fig. 1a is shown in Fig. 1c, which shows that the Ta element is the unique substance on the surface of Ta-coated SS316L, and there are no peaks indicating SS316L, which means that the thickness of Ta-coating is thicker than that of the penetration of electron.

Fig. 1d is the cross-sectional micrograph of SS316L with Ta-coating, in which the blue line indicates tantalum, the red line iron, green chromium, and purple line nickel. Observing Fig. 1d, it shows an obvious boundary between the basal material and the Ta-coating; the connecting surface is tight, and the thickness of Ta-coating is about 3 μm.

3.1.2. XRD characterization of uncoated and Ta-coated SS316L

Fig. 2 shows the XRD results for uncoated and Ta-coated SS316L. It is clear that SS316L has a face centered cubic (FCC) structure shown in Fig. 2a, and Ta-coated SS316L has a body centered cubic (BCC) structure seen in Fig. 2b. Comparing Fig. 2a with Fig. 2b, it is seen that there is no peak of SS316L in Fig. 2b, which means that the penetration of X-rays is less than the thickness of Ta-coating, and the result is well coincident with the result obtained in Fig. 1. Besides observing Fig. 2b, it can be also seen that the (1 1 0) diffraction peak is the strongest, so the growth orientation of Ta is mainly in the ⟨1 1 0⟩ direction.

3.2. Potentiodynamic properties

Fig. 3 is the potentiodynamic polarization testing results of uncoated and Ta-coated SS316L in 0.5 mol dm^{-3} H_2SO_4 electrolyte at 70 °C. It can be seen that potentiodynamic polarization curves of uncoated SS316L and Ta-coated SS316L are different from each other. The former curve can be divided into six regions [16]. Curve AB stands for cathode polarization, in which the current density decreases with the increasing potential, the liberating speed of H_2 is faster than the dissolving speed of the metal, and the main electromechanical process in this region is the liberation of H_2. Curve BC is the anode polarization region, and during this period, the current density increases with the potential increased, thus dissolving the metal faster than the liberating of H_2, thus, the main electromechanical process is the dissolving of the base metal. With the strengthening of anode polarization, when the potential exceeds that of C point, current density decreases with increasing potential, so curve CD shows the transitional region from activation to passivation. With potential exceeds that of D point, current density increases again along with increasing potential; the main reason resulting in increasing current density is the transformation of iron or chromium from bivalence to trivalency. When potential exceeds that of E point, current density keeps stable, so curve EF indicates passive region; during this period, passive film is obtained on the surface of SS316L owning to high content of chromium (16.45%), which can well prevent metal from dissolving. As soon as potential value is beyond that of F point, current density increases quickly with increasing potential, which is named transpassive region, and the main electromechanical process is the liberation of O_2 and destruction of passive film [16,17].

Potentiodynamic polarization curve of Ta-coated SS316L can be divided into four regions: cathode region (curve ab), anode region (curve bc), passive region (curve cd) and transpassive region (curve de) [17]. There is no obvious transitional region from activation to passivation, and the passive region is more stable for Ta-coated SS316L.

In addition, it can be seen in Fig. 3 that the open circuit potential of SS316L is −304.560 mV versus SCE, and the OCP of Ta-coated SS316L is −289.282 mV versus SCE, so increased potential can well protect SS316L from corrosion.

Based on the linear polarization data and Eq. (1), polarization resistances of uncoated and Ta-coated SS316L in 0.5 mol dm^{-3} H_2SO_4 at 70 °C can be obtained, and detailed polarization parameters such as corrosion current density, polarization resistance and Tafel slopes of the anodic and cathodic reactions can be seen in

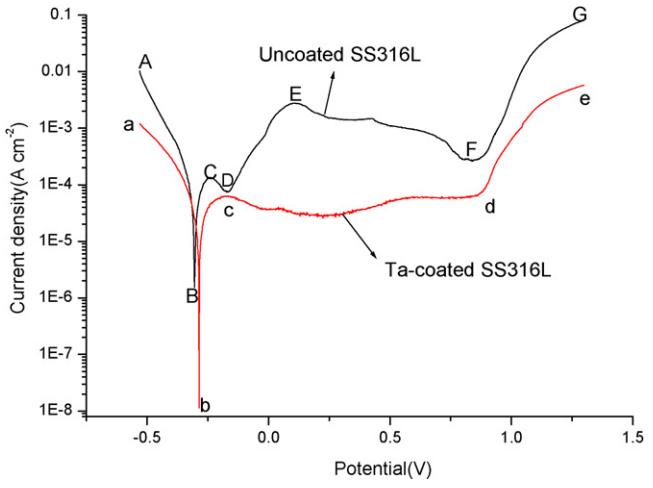

Fig. 3. Potentiodynamic polarization testing results of uncoated and Ta-coated SS316L.

Table 2
Polarization parameters of uncoated and Ta-coated SS316L in 0.5 mol dm^{-3} H_2SO_4 at 70 °C.

Metal	β_a (mV)	β_c (mV)	i_{corr} (μA cm^{-2})	E_{corr} (mV)	R_p (Ω cm^2)
Uncoated SS316L	99.247	70.883	44.61	−304.560	403
Ta-coated SS316L	44.778	40.635	9.25	−289.282	1002

Table 2

$$R_p = \frac{\beta_a \beta_c}{2.3 i_{corr}(\beta_a + \beta_c)} \quad (1)$$

where β_a, β_c, i_{corr}, and R_p are Tafel slopes of the anodic and cathodic reactions, corrosion current density and polarization resistance respectively [18].

It is clear that the corrosion current densities of uncoated SS316L is 44.61 μA cm^{-2} versus 9.25 μA cm^{-2} for Ta-coated SS316L, a decrease of about 5 times, which shows lower corrosion rate for Ta-coated SS316L. It can also be seen that the polarization resistances of uncoated SS316L is 403 Ω cm^2 versus 1002 Ω cm^2 for Ta-coated SS316L, an increase of about twice, showing better anticorrosion property with Ta-coating.

Fig. 4a is SEM picture of uncoated SS316L after potentiodynamic testing, indicating uncoated SS316L is corroded mainly on grain boundary; the reason is that there is chromium carbides ($Cr_{23}C_6$) precipitated at the grain boundaries, which consumes chromium in boundary region, and results in the decrease of chromium content in these areas, consequently, the potential at the grain boundaries is lower than that at interior grain, corrosion microbattery being generated, so grain boundary as anode of microbattery will firstly be corroded [19]. Moreover, there is also some pitting corrosion, due to the formation of "big cathode/small anode" galvanic couples, which are caused by pin-holes or destruction of passivating film on the surface of SS316L. Observing Fig. 4b, there is no obvious corrosion phenomenon for Ta-coated SS316L, so Ta-coating can well play an anticorrosion role on surface modification of SS316L.

3.3. Potentiostatic properties in simulative working environment

Considering different working potentials (the potential of anode is about −0.1 V versus SCE, and the potential of cathode is about 0.6 V versus SCE) for bipolar plates in PEMFC [20], potentiostatic tests with simulative working environment of PEMFC for anode and cathode plates were conducted in this paper. OCPs of uncoated and Ta-coated SS316L are −304.560 mV and −289.282 mV respectively, the simulative anode potential is anodic to uncoated SS316L and Ta-coated SS316L, and the simulative cathode potential is also anodic to both uncoated and Ta-coated SS316L.

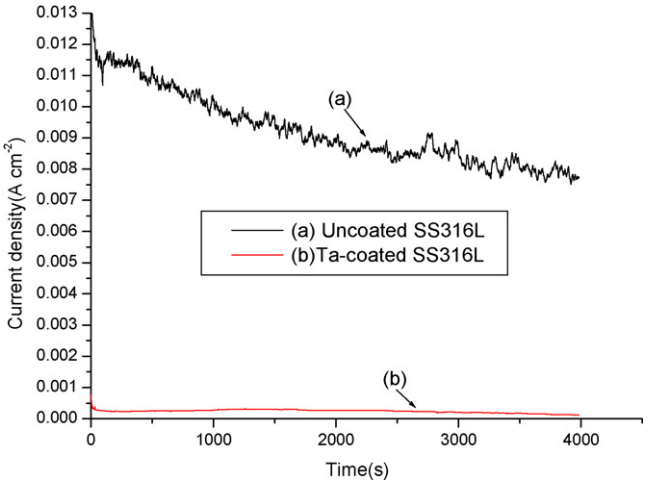

Fig. 5. Potentiostatic testing results in simulative anode condition: (a) uncoated SS316L, (b) Ta-coated SS316L.

Fig. 5 is potentiostatic testing results of uncoated and Ta-coated SS316L at simulative anode working conditions. It can be seen in Fig. 5 that the current densities for both uncoated and Ta-coated SS316L are positive, the current density of uncoated SS316L is about 9×10^{-3} A cm^{-2}, the current density of Ta-coated SS316L is stabilized at about 2×10^{-4} A cm^{-2}, an reduction of 45 times, so Ta-coating can well reduce corrosion current density when Ta-coated SS316L is used as anode in PEMFC.

Fig. 6 are the potentiostatic tesing results in simulative cathode condition for uncoated and Ta-coated SS316L, which shows that both current densities of uncoated and Ta-coated SS316L are positive, the current density of uncoated SS316L is stabilized at about 8.9×10^{-4} A cm^{-2}, Ta-coated SS316L 6.5×10^{-8} A cm^{-2}, a dramatic reduction, so Ta-coating can significantly protect SS316L from corrosion, and Ta-coated SS316L can be well used as cathode in PEMFC.

Fig. 7 shows SEM pictures of both uncoated and Ta-coated SS316L after potentiostatic polarization in simulative anode and cathode working conditions. Fig. 7a and b are SEM pictures of uncoated SS316L after potentiostatic polarization at simulative anode working potential, compared with Fig. 4a, it can be seen that there is no obvious corrosion phenomena for uncoated SS316L after potentiostatic polarization. In order to observe corrosion situation of uncoated SS316L in detail, micrograms zoomed in about 12 times from Fig. 7a and b are shown in Fig. 7c and d, the corrosion phenomena is obvious and mainly controlled by pitting corrosion for uncoated SS316L in both anode and cathode simulative working conditions, but the extent of corrosion for uncoated

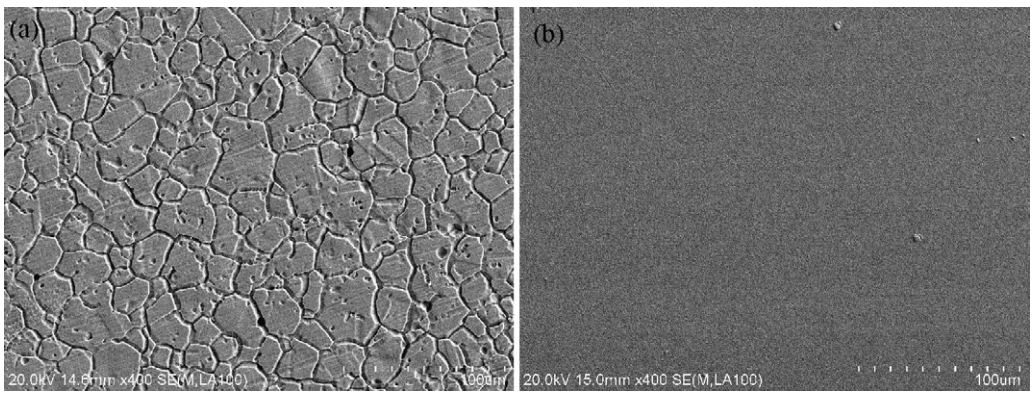

Fig. 4. SEM micrograms of uncoated (a) and Ta-coated (b) SS316L after potentiodynamic testing.

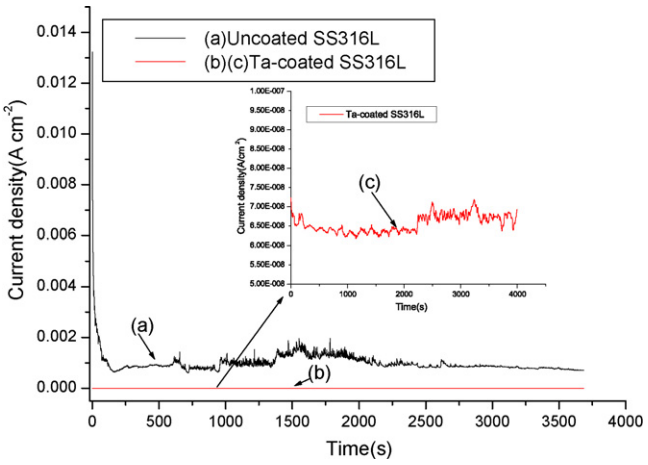

Fig. 6. Potentiostatic testing results in simulative cathode condition: (a) uncoated SS316L, (b) and (c) Ta-coated SS316L.

SS316L in anode simulative working condition is severer than that in simulative cathode working condition, which is consistent with potentialstatic polarization testing results (for uncoated SS316L, corrosion current density is 9×10^{-3} A cm^{-2} in simulative anode working condition versus 8.9×10^{-4} A cm^{-2} in simulative cathode working condition) obtained from Fig. 5a and Fig. 6a. Fig. 7e and f are corrosion micrograms of Ta-coated SS316L after potentiostatic polarization in both anode and cathode simulative working conditions, showing no obvious corrosion compared with Fig. 1a, which also shows that the corrosion phenomena of Ta-coated SS316L in both anode and cathode simulative working conditions are not serious compared with Fig. 7c and d. It can also be found that the extent of corrosion for Ta-coated SS316L in simulative anode working condition is severer than that in simulative cathode working condition, which is also consistent with results (for Ta-coated SS316L, corrosion current density is 2×10^{-4} A cm^{-2} in simulative anode working conditions versus 6.5×10^{-8} A cm^{-2} in simulative cathode working conditions) obtained from Fig. 5b and b.

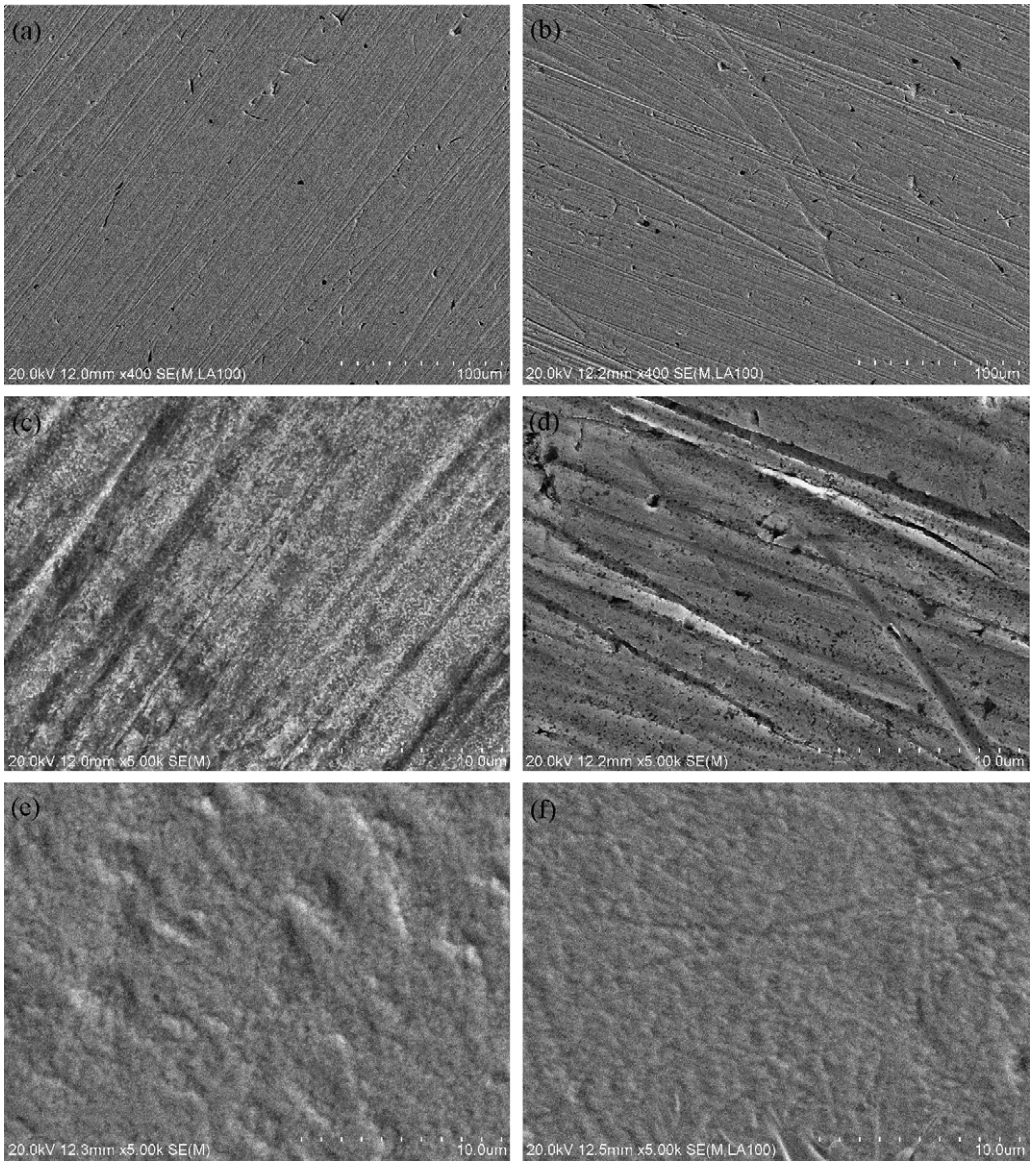

Fig. 7. SEM pictures of uncoated and Ta-coated SS316L after potentiostatic polarization in simulative working conditions, (a) uncoated SS316L at anode, (b) uncoated at cathode, (c) megascopic picture from (a), (d) megascopic picture from (b), Ta-coated SS316L at anode, (d) Ta-coated SS316L at cathode.

4. Conclusions

Metallic Ta is well coated on the surface of SS316L, homogeneously distributed on the surface, mainly grows in the ⟨1 1 0⟩ direction, and the thickness is about 3 μm. The OCPs of uncoated and Ta-coated SS316L are −304.560 mV and −289.282 mV versus SCE respectively. SS316L with Ta-coating has better anticorrosion property than that of uncoated SS316L, and corrosion current density is 44.61 $\mu A\,cm^{-2}$ for uncoated SS316L versus 9.25 $\mu A\,cm^{-2}$ for Ta-coated SS316L, a decrease of about 5 times.

In potentialstatic polarization testing with simulative working condition, the current densities of both uncoated and Ta-coated SS316L in anode and cathode environment are positive, but current densities in cathode environment are smaller than those in anode environment no matter uncoated or Ta-coated SS316L, which also can be testified by SEM microgram analysis, so Ta-coating can prevent SS316L from corrosion, and can well be considered as a method to modify SS316L used in PEMFC.

References

[1] R. Jiang, D. Chu, J. Power Sources 93 (2001) 25.
[2] S.S. Hsieh, S.H. Yang, J.K. Kuo, C.F. Huang, H.H. Tsai, Energy Convers. Manage. 47 (2006) 1868.
[3] I. Bar-On, R. Kirchan, R. Roth, J. Power Sources 109 (2002) 71.
[4] H. Tsuchiya, O. Kobayashi, Int. J. Hydrogen Energy 29 (2004) 985.
[5] A. Hermann, T. Chaudhuri, P. Spagnol, Int. J. Hydrogen Energy 30 (2005) 1297.
[6] H. Tawfik, Y. Hung, D. Mahajan, J. Power Sources 163 (2007) 755.
[7] M.H. Fronk, R.L. Borup, J.S. Hulett, B.K. Brady, K.M. Cunningham, US6372376B1.
[8] L.A. Dobrzanski, K. Lukaszkowicz, A. Zarychta, L. Cunha, J. Mater. Process. Technol. 164–165 (2005) 816.
[9] K. Shah, Y. Zhu, J.O. Rroh, O. Popoola, Surf. Eng. 17 (5) (2001) 405.
[10] M.A. Lucio Garcia, M.A. Smit, J. Power Sources 158 (2006) 397.
[11] Y. Wang, D.O. Northwood, J. Power Sources 163 (2006) 500.
[12] S.S. Hsieh, C.L. Feng, C.F. Huang, J. Power Sources 163 (2006) 440.
[13] L. Ma, S. Warthesen, D.A. Shores, J. New Mater. Electrochem. Syst. 3 (2000) 221.
[14] D.R. Hodgson, B. May, P.L. Adcock, D.P. Davies, J. Power Sources 96 (2001) 233.
[15] Y. Li, L. Qu, F. Wang, Corros. Sci. 45 (2003) 1367.
[16] Y. Wang, D.O. Northwood, J. Power Sources 165 (2007) 293.
[17] D. Yang, Z. Shen, Metal Corrosion, Metallurgy Industry Press, 2003, p.58.
[18] D.A. Jones, Principles and Prevention of Corrosion, first ed., Macmillan, New York, 1992, p. 147.
[19] Y. Wang, D.O. Northwod, J. Hydrogen Energy 32 (2007) 895.
[20] H. Wang, J.A. Turner, J. Power Sources 128 (2004) 193.